ACS APPLIED MATERIALS & INTERFACES

Research Article

www.acsami.org

Preparation of Nitrogen-Doped Carbon Nanotubes with Different Morphologies from Melamine-Formaldehyde Resin

Yi Yao,[†,‡] Bingqing Zhang,[§,∥] Jingying Shi,[†,§] and Qihua Yang*[,†]

[†]State Key Laboratory of Catalysis, Dalian Institute of Chemical Physics, Chinese Academy of Sciences, 457 Zhongshan Road, Dalian 116023, China

[‡]Graduate School of the Chinese Academy of Sciences, Beijing 100049, China

[§]State Key Laboratory of Catalysis, Dalian National Laboratory for Clean Energy, Dalian Institute of Chemical Physics, Chinese Academy of Sciences, Dalian, 116023, P. R. China

[∥]The Key Laboratory of Fuel Cell Technology of Guangdong Province and The Key Laboratory of New Energy Technology of Guangdong Universities, School of Chemistry and Chemical Engineering, South China University of Technology, Guangzhou, Guangdong 510641, P. R. China

Supporting Information

ABSTRACT: We report a facile method for the synthesis of nitrogen-doped carbon nanotubes (NCNTs) from melamine-formaldehyde (MR) resin using $FeCl_3$ or supported $FeCl_3$ as catalysts. The growth of NCNTs follows a decomposition−reconstruction mechanism, in which the polymer precursor would totally gasify during pyrolysis process and then transformed into carbon nanotubes. The morphology of the NCNTs could be adjusted via applying different catalyst supports and three kinds of carbon nanotubes with outer-diameter of 20−200 nm and morphologies of either bamboo-like or hollow interiors were obtained. Nitrogen atoms in the materials were mainly in the form of pyridinic and quaternary form while the formation of iron species strongly depended on the interaction between iron precursor and organic carbon/nitrogen sources. All MR resin derived NCNTs are efficient toward oxygen reduction reaction (ORR). NCNTs prepared using $FeCl_3$ as catalyst showed the highest ORR activity with half-wave potentials of −0.17 V, which is comparable with commercial Pt/C. This is probably because of a close contact between MR resin and iron precursor could enhance the iron-ligand coordination strength and thus steadily improve the performance of the catalyst.

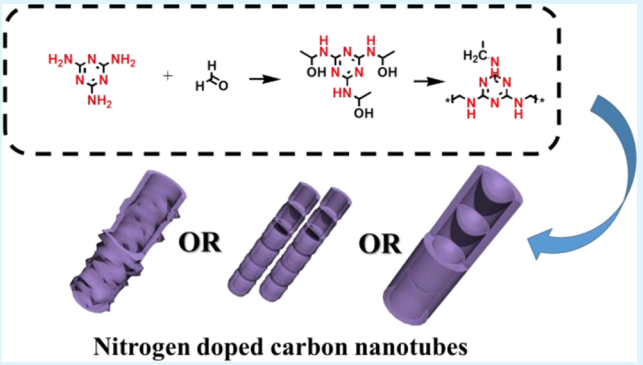

KEYWORDS: *carbon nanotubes, nitrogen doping, oxygen reduction reaction*

INTRODUCTION

After the report from Iijima on the observation of multiwalled carbon nanotubes in 1991,[1] the research on both fundamental aspects and commercial applications of this material has been lasting for decades.[2] Carbon nanotubes could be defined as "rolled" graphene sheets with cylinder structures. Besides high crystalline and intrinsic conductivity of carbon materials, CNTs possess large surface areas and superior mass-transfer and mechanical properties.[3] The doping of heteroatoms, such as nitrogen, phosphor, sulfide, boron, and etc., further enriched the chemistry of this material especially in catalysis, because the heteroatoms with different electron configurations would attract or repel electrons in neighboring carbon atoms, generating active sites for several kinds of reactions.[4−6] Recently extensive interest have been initiated by nitrogen-doped CNTs. Reports on better performance in oxygen reduction reactions and lithium ion anchoring abilities over pure carbon materials have been confirmed by different researchers, showing its potential in both energy conversion and storage field.[7]

The preparation of carbon nanotubes is the very first task in front of the researchers, for MWCNTs were originally obtained via arc evaporation by using a graphite rod as the electrode in little amount. The development of chemical vapor deposition (CVD) provided a much feasible way to synthesize carbon nanotubes with desired quality in large amount.[2] Carbon sources in small organic molecule forms like hydrocarbons[8] and alcohols like methane,[9] ethanol,[10] and etc. were used to grow CNTs on metal nanoparticle loaded substrates such as silica or silicon carbide.[11] Nitrogen atoms could be introduced during the process by mixing the carbon resource with or merely using raw materials like gasified cyanamide,[12] melamine,[13] pyridine,[14]

Received: February 8, 2015
Accepted: March 19, 2015
Published: March 19, 2015

DOI: 10.1021/acsami.5b01233
ACS Appl. Mater. Interfaces 2015, 7, 7413−7420

acetonitrile,[15] and etc.[16−18] The thermodynamic parameters should be carefully controlled otherwise the difference in the activity of heteratoms would lead to the formation of defective products. In addition, because of this difference, unlike post-treated NCNTs (CNTs treated with ammonia, for example),[19] the nitrogen-doped CNTs prepared in this way usually has a bamboo like morphology. The restricts on equipment and control of the reaction condition motivated researchers to design more feasible synthesis routines to obtain NCNTs. Using nitrogen containing polymers as the precursor would be a solution to the problem. Solid precursors could be transformed into NCNTs via a decomposition−reconstruction mechanism—they were first gasified into small fragments via pyrolysis and then assembled in to one-dimensional tubular structure on the metal catalysts. In other words, the essential mechanism is the same with CVD method, but cheap raw materials and simple equipment could be enough for the procedure and careful control of the condition is not necessary. So far, both CNTs and NCNTs prepared from carbon containing polymers such styrene−divinylbenzene copolymer resin[20] and polymers with prebonded nitrogen atoms like g-C3N4[21] and Fe-containing ZIFs[22−24] have already been reported.

Herein, we report the synthesis of nitrogen-doped carbon nanotubes from melamine formaldehyde resin (MF resin). By adjusting the catalyst support, the morphology of the product could be slender bamboo-like, thick bamboo-like, and hollow tubes. It was found that the dispersion of iron precursors would largely influence the size of iron particles formed during the pyrolysis process and thus alter the final morphology of the product. All three kinds of carbon nanotubes showed good activities toward oxygen reduction reaction and the differences among the materials shed a light on the influence of preparation procedure toward the activities.

EXPERIMENTAL SECTION

Materials and Characterizations. Melamine, formaldehyde solution, magnesium oxide, iron(III) chloride hexahydrate, and sodium hydroxide were purchased from Sinopharm Chemical Reagent Co.; melamine formaldehyde foam was provided by SINOYQX (Sichuan, China), and absolute ethanol was purchased from Kemiou Chemical Reagent Co. All chemicals were used as received without further purification.

The high-resolution scanning electron microscopy (HRSEM) was performed on Hitachi S-5500 scanning electron microscope operating at an acceleration voltage of 30 kV. The transmission electron microscopy (TEM) was undertaken using a Hitachi HT-7700 at an acceleration voltage of 100 kV. The samples were placed onto an ultrathin carbon film supported on a copper grid. The powder X-ray diffraction data were collected on a Rigaku D/Max2500PC diffractometer with Cu Kα radiation (λ = 1.5418 Å) over the 2θ range of 5−80° with a scan speed of 5 deg/min at room temperature. The nitrogen sorption experiments were performed at 77 K on a Micromeritics ASAP 2020 system. Prior to the measurement, the samples were degassed at 140 °C for 6 h. The Raman spectra were taken with Renishaw InVia confocal Raman microscope

Synthesis of Fe@MgO Catalysts. Five grams of Iron(III) chloride hexahydrate was dissolved in 100 mL of ethanol and then 10 g of MgO powder was added under vigorous stirring. The reaction was exothermic and brownish powder product was obtained after cooling, filtering, and drying.

Synthesis of Melamine Formaldehyde Resin. Melamine formaldehyde resin was prepared via the reaction of melamine and formaldehyde first under alkaline conditions and then condenses in acid. The detailed procedure is as follows: 4 g of melamine was mixed with 10 mL of deionized water and 8 mL of formaldehyde solution (~37% wt.). The pH of the aqueous suspension was adjusted to 10 via adding 1 M NaOH solution. The reaction was carried out under vigorous stirring at 75 °C for 30 min and a clear solution was obtained. The soluble precursor was cooled to ambient temperature, and then 1 mL of acetic acid was added. The solution was stirred overnight and the white precipitate of melamine formaldehyde resin was separated via either centrifugation or filtration. The product was dried under 100 °C.

Synthesis of Slender Bamboo-like NCNTs (S-B-NCNTs). In a typical synthesis 0.75 g of Fe@MgO catalyst was mixed with 3 g of melamine formaldehyde powder, the mixture was grounded and transferred into a crucible. The precursor was stabilized in air under 200 °C for 3 h, and then pyrolyzed in nitrogen at 950 °C for 1 h. The heating rate was set to 10 °C/min and the gas flow was 20 mL/min. Black powder of S-B-NCNTs was obtained after cooling to room temperature. The exposed metal and metal oxide was removed via stirring the product in 1 M HCl at 80 °C for 8 h. A secondary heat treatment was conducted under the same condition with the first pyrolysis procedure before characterization.

Synthesis of Thick Bamboo-like NCNTs (T-B-NCNTs). The clear solution made from the reaction of melamine and formaldehyde was prepared in a similar way as described in the Synthesis of Melamine Formaldehyde Resin. After cooling down the clear solution from 75 °C to room temperature, 0.5 g of iron(III) chloride hexahydrate (dissolved in 10 mL deionized water) was added. The solution soon turned into reddish brown and yellowish brown precipitate was obtained after stirring overnight (Supporting Information Figure S1). The product was collected via either centrifugation or filtration and then dried under 100 °C. The air stabilization, pyrolysis, acid treatment, and secondary heat treatment procedures were the same with S-B-NCNTs.

Synthesis of Thick Hollow NCNTs (T-H-NCNTs). The clear solution made from the reaction of melamine and formaldehyde was prepared in a similar way as described in the Synthesis of Melamine Formaldehyde Resin. After cooling down the clear solution from 75 °C to room temperature, the melamine formaldehyde foam with size of 1 cm × 1 cm × 1 cm cubes was added. The mixture was stirred for at least 1 h; 0.5 g of iron(III) chloride hexahydrate (dissolved in 10 mL deionized water) was added afterward and the solution soon turned into reddish brown. Finally yellowish brown cubes and precipitate was obtained after stirring overnight. The cubes were picked out and then dried at 100 °C. The air stabilization, pyrolysis, acid treatment, and secondary heat treatment procedures were the same with S-B-NCNTs.

Electrochemical Measurements. Electrochemical measurements were performed using a CHI Electrochemical Station (Model 730D) in a three-electrode electrochemical cell at room temperature. Platinum foil and a saturated calomel electrode (SCE) were using as the counter and reference electrode, respectively. The catalyst layer on the glassy carbon electrode was prepared as follows. A mixture with 5 mg of NCNTs catalyst, 1 mL of absolute ethanol, and 50 μL of Nafion (5 wt %, Du Pont Corp.) was prepared using sonication. Thirty microliters of ink was dropped onto the glassy carbon disk, which was then left to dry in air at room temperature, to yield a catalyst loading of ~750 μg cm^{-2}. For comparison, the loading of commercial Pt/C (20 wt %, Johnson Matthey) catalyst was 25 μg Pt cm^{-2}.

In the rotating disk electrode (RDE) tests, the linear sweep voltammograms (LSVs) were recorded in O_2 saturated 0.1 M KOH solution and the electrode potential was scanned between −0.8 and 0.2 V with a scan rate of 10 mV/s at a fixed rotating speed of 1600 rpm. In the accelerated durability test the cyclic voltammograms scanning was measured in naturally aerated 0.1 M KOH electrolyte under the potential between −0.5 and 0.1 V (vs SCE); then polarization curves was taken in O2-saturated 0.1 M KOH electrolytes with the scan rate of 10 mV/s and rotation rate of 1600 r/min. The electron transfer number of T-B-NCNTs was calculated according to the Koutecky−Levich equation

DOI: 10.1021/acsami.5b01233
ACS Appl. Mater. Interfaces 2015, 7, 7413−7420

Scheme 1. Schematic Illustration of the Preparation of Nitrogen-Doped Carbon Nanotubes from Melamine-Formaldehyde Resin in the Presence of $FeCl_3$, Mixture of MgO and $FeCl_3$, or MgO-Supported $FeCl_3$

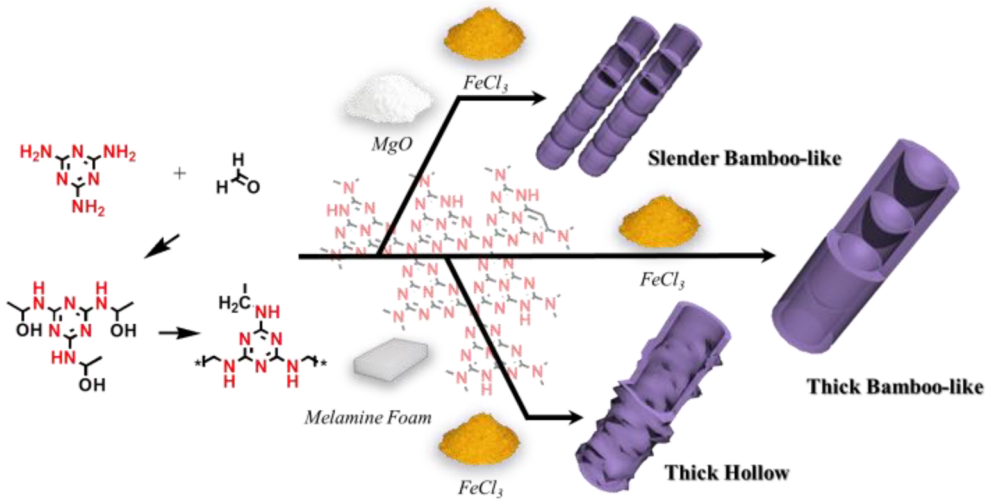

$$\frac{1}{j} = \frac{1}{j_l} + \frac{1}{j_k} = \frac{1}{B\omega^{1/2}} + \frac{1}{j_k}$$

$$B = 0.62nFD_0^{2/3}\nu^{-1/6}C_0$$

$$j_k = nFkC_0$$

where j is the measured current density, j_l is the diffusion-limiting current densities, j_k is the kinetic current density, F is the Faradaic constant (96 485 C mol^{-1}), D_0 is the O_2 diffusion coefficient 0.1 M KOH (1.9×10^{-9} m^2 s^{-1}), C_0 is the O_2 saturation concentration in 0.1 M KOH (1.21 mol m^{-3}), ν is the kinematic viscosity in 0.1 M KOH (1×10^{-6} m^2 s^{-1}), ω is the angular velocity of the disk ($\omega = 2\pi N$, N is the linear rotation rate), and k is the electron transfer rate constant. The number of electrons transferred (n) and the kinetic-limiting current (j_k) can be obtained from the slope and intercept of the Koutecky–Levich plots ($1/j$ versus $\omega^{-1/2}$).

RESULTS AND DISCUSSION

Nitrogen-doped carbon nanotubes were synthesized using melamine formaldehyde resin with approximately equal nitrogen to carbon ratio as a precursor, which has been usually used to prepare nitrogen-doped carbon materials under high temperature.[25−27] The synthesis procedure is outlined in Scheme 1. The samples synthesized in the presence of MgO supported $FeCl_3$, $FeCl_3$, and melamine foam/$FeCl_3$ were denoted as S-B-NCNTs, T-B-NCNTs, and T-H-NCNTs, respectively. The cross-linked polymer would form an ordered graphitic structure around 500−600 °C but decompose into small gaseous molecules such as nitrogen and cyano fragments when temperature was risen to higher than 700 °C,[28] which could serve as carbon and nitrogen sources to form nitrogen-doped carbon materials. To testify the proposed possibility of growth for nitrogen-doped CNTs the mixture of MgO supported iron chloride and air stabilized melamine-formaldehyde resin was heat treated at 750, 850, and 950 °C. The TEM pictures show that carbon nanotubes with a thick wall could be formed at 750 °C (Supporting Information Figure S2). The produced CNTs had a hollow morphology, but the length of each tube was only several hundreds of nanometers. In addition to CNTs, other amorphous carbon materials could also be observed. Further raising the temperature to 850 °C, bamboo-like CNTs with wide diameter distributions could be observed (Supporting Information Figure S3). The amorphous carbon materials coexist with CNTs. When pyrolysis temperature reached to 950 °C, the products were mainly carbon nanotubes with bamboo-like morphology constructed with small hollow cells, which could commonly be observed in CNTs prepared with high nitrogen content (Figure 1a, b and Supporting Information Figure S4a, b). The lengths and outer-diameters of this bamboo-like CNTs were ∼2 um and ∼20 nm, respectively. Iron nanoparticles with similar particle size to the tube diameter scattered inside the slender-bamboo like-NCNTs (S-B-NCNTs). Considering the ordinary growth mechanism of CNTs, we believe the iron particle catalyzed the growth process and their size determined the final morphology of the NCNTs.[29]

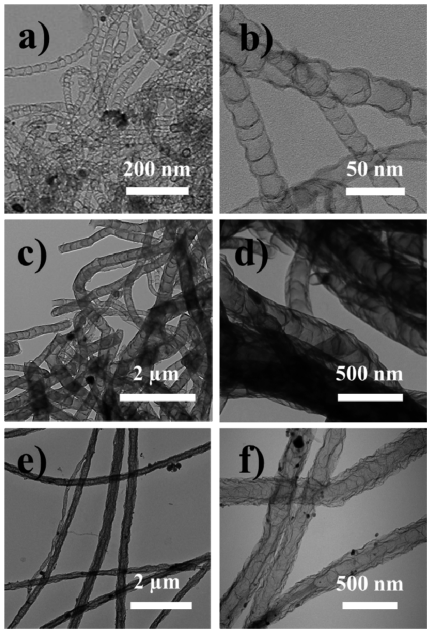

Figure 1. TEM pictures of (a, b) S-B-NCNTs prepared from mixture of MgO supported $FeCl_3$ and MF resin at 950 °C, (c, d) T-B-NCNTs prepared from $FeCl_3$/MF resin at 950 °C, and (e, f) T-H-NCNTs prepared from $FeCl_3$/MF resin/commercial melamine foam at 950 °C under different magnitudes.

DOI: 10.1021/acsami.5b01233
ACS Appl. Mater. Interfaces 2015, 7, 7413−7420

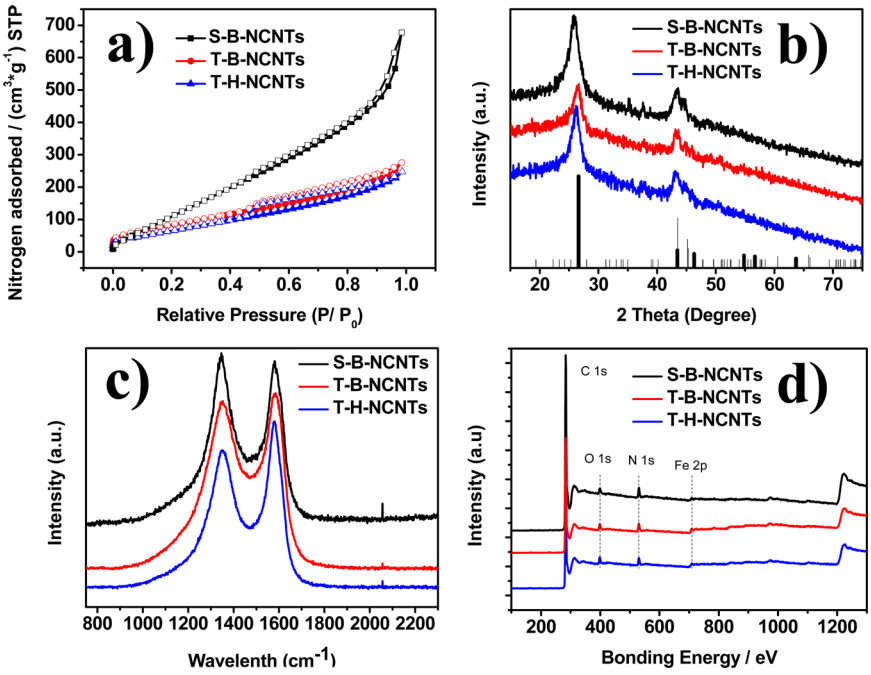

Figure 2. (a) Nitrogen adsorption−desorption isotherm curves, (b) XRD patterns (−, graphitic carbon; −, iron carbide), (c) Raman spectra, and (d) XPS surveys of NCNTs prepared via different procedures.

In the next step, we adjusted the synthesis procedure by removing MgO, for the dispersion of iron would be different without a support which should probably change the morphology of the CNTs finally obtained. When solvated $FeCl_3$ was added into the solution of melamine resin oligomers, Fe^{3+} ions were directly attached to the oligomers of melamine resin and the clear solution turned rapidly into brownish red. Finally the mixture of iron precursor and polymer participated as a yellowish brown solid. Heat treatment at 950 °C under the same preparation conditions to S-B-NCNTs resulted in carbon nanotubes T-B-NCNTs, thick-bamboo like-NCNTs, with a diameter of ∼200 nm (Figure 1c, d). As we expected larger iron particles were identified inside the CNTs. The above results suggest that the differences in the aggregation status of the iron catalyst play an important role in the growth mechanism. When no support was used, iron salt loaded on the polymer was much easier to aggregate during the heat treatment process, thus larger metal particles were formed. To further confirm the assumption, we embedded iron-containing melamine resin precursor into commercial melamine foam with a pore size of around 100 μm.[22] Since the oligomers were soluble before adding $FeCl_3$, it could easily penetrate into the foam and finally consolidated as bulk blocks. Thick-Hollow-NCNTs (T-H-NCNTs) derived by treating this precursor under similar conditions to S-B-NCNTs at 950 °C were with wrinkled wall, large iron particles (∼100 nm) inside the tube and small ones (∼20 nm) around the wall. Magnified picture of the local structure indicates that the wall was constituted with several layers of wrinkled lamellate graphitic carbon. We suppose that on the formation of these CNTs large iron particles gradually collapsed or transformed during the pyrolysis. Larger iron particles served as catalysts for the formation of the main structure and small ones participated into the formation of the wrinkled graphitic structures around, for only on this sample small iron particles were observed on the wall of CNTs. The uniformity of three kinds of materials was also confirmed via scanning electron microscopic pictures (Supporting Information Figure S4).

Nitrogen adsorption/desorption measurement was performed and the results are shown in Figure 2a. All samples were heated in excess diluted sulfuric acid to remove metal/metal oxides outside the materials before the test. The S-B-NCNTs showed a BET surface area of 564 m^2/g, which is much larger than ordinary commercial products with a BET surface area of about 150−250 m^2/g. The BET surface area for T-B-NCNTs and T-H-NCNTs was 310 and 253 m^2/g respectively, which are comparable to the materials prepared with similar procedure. X-ray diffraction was performed on the three samples and from the diffraction patterns (Figure 2b) two set of peaks could easily be identified as features of graphitic carbon (JCPDS-PDF-75-2078) and iron carbide (JCPDS-PDF-71-1174). Small difference in the location of the peaks at about 26.6° indicates the difference of *d*-spacing between adjacent carbon layers. According to the Bragg's Equation, the d-space of S-B-NCNTs, T-B-NCNTs, and T-H-NCNTs was 3.43, 3.35, and 3.39 Å. The intensity of D and G band on the Raman spectra of carbon materials was used to determine the defect density and graphitic degree of the material (Figure 2c). The I_G/I_D value goes with the order T-H-NCNTs (1.21) > T-B-NCNTs (1.05) > S-B-CNTs (0.96). Usually there are two factors that could increase the intensity of D band, one is the incorporation of heteroatoms (nitrogen here) and the other is curvature of the CNTs, thus it is not surprise the sample with the smallest diameter owns the highest amount of defects. Nitrogen and iron content in all materials were determined by element analysis and ICP (Table 1). XPS was also performed and on the survey results (Figure 2d) we could easily identify the feature peaks of C 1s, O 1s, N 1s and Fe 2p. The fine structure of the XPS spectra of N 1s was investigated. It is of particular interest because the nitrogen atoms embedded in the matrix of carbon play an important role in catalysis processes such as oxygen reduction reaction, oxygen evolving reaction,

DOI: 10.1021/acsami.5b01233
ACS Appl. Mater. Interfaces 2015, 7, 7413−7420

Table 1. Nitrogen and Iron Content of the Catalysts after Treating (Acid Resining and Second Pyrolysis)[a]

sample	N (m/m %)	N after 2nd pyrolysis (m/m %)	Fe after 2nd pyrolysis (wt %)
S-B-NCNTs	3.91	3.29	11.4
T-B-NCNTs	3.88	3.33	9.2
T-H-NCNTs	3.36	3.13	8.7

[a]The 2nd pyrolysis procedure would remove some nitrogen contents from the materials.

hydrogen evolving reaction and etc.[6] N 1s peaks of three materials showed similar shapes, they could all be divided into the signals of pyridinic(~397 eV), pyrrolic(~398 eV), quaternary(~400 eV), and oxidized(~403 eV) nitrogen atoms.[6] Nearly half of the nitrogen atoms in all three kinds of materials were mainly in the form of quaternary N, which is embedded into the NCNTs and substituting carbon atoms within the rolled-graphitic plane. The other half nitrogen atoms are mainly pyridinic and pyrrolic N, which could be coordinated with transition metal ions to produce metal−N4 centers and serve as active site for oxygen reduction reaction. Only slight differences of the relative content of nitrogen species were observed (Figure 3a−c and Supporting Information Table S1). The result was not surprising because three kinds of materials were formed under the same temperature applying the same nitrogen/carbon sources so nitrogen atoms should be incorporated in the same manner. But the situation was quite different when it came to the XPS of Fe 2p (Figure 3d−f and Supporting Information Table S2). According to the peak fitting results, iron atoms in the as prepared NCNTs were mainly in the form of Fe^{2+} (~709 eV), Fe^{3+} (~711 eV), and metallic Fe^0 (~706 eV).[30] The reduced form of iron (Fe^0) in T-B-NCNTs was much less than that in other NCNTs. This phenomenon was interesting for there were no significant differences in the iron precursors used in the synthesis procedures either. The most remarkable distinction should be the extent of interaction between Fe^{3+} and MF resin oligomers. During the preparation of T-H-NCNTs Fe^{3+} was directly bonded to the polymer, while for the other two materials all/part of the MR resin were precondensed and interacted with iron precursors via simply mixing. Thus, we suppose that the formation of different iron species in the products is probably due to the different catalyst dispersion degree and the interaction between Fe^{3+} and MF resin oligomers might help the iron species to hold a higher valence during the pyrolysis, forming structures, such as iron carbide or Fe^{2+}/Fe^{3+}-N4 centers.[31]

Oxygen reduction reaction is one of the key steps in chemical to electrical energy conversion. The slow kinetic of the reaction

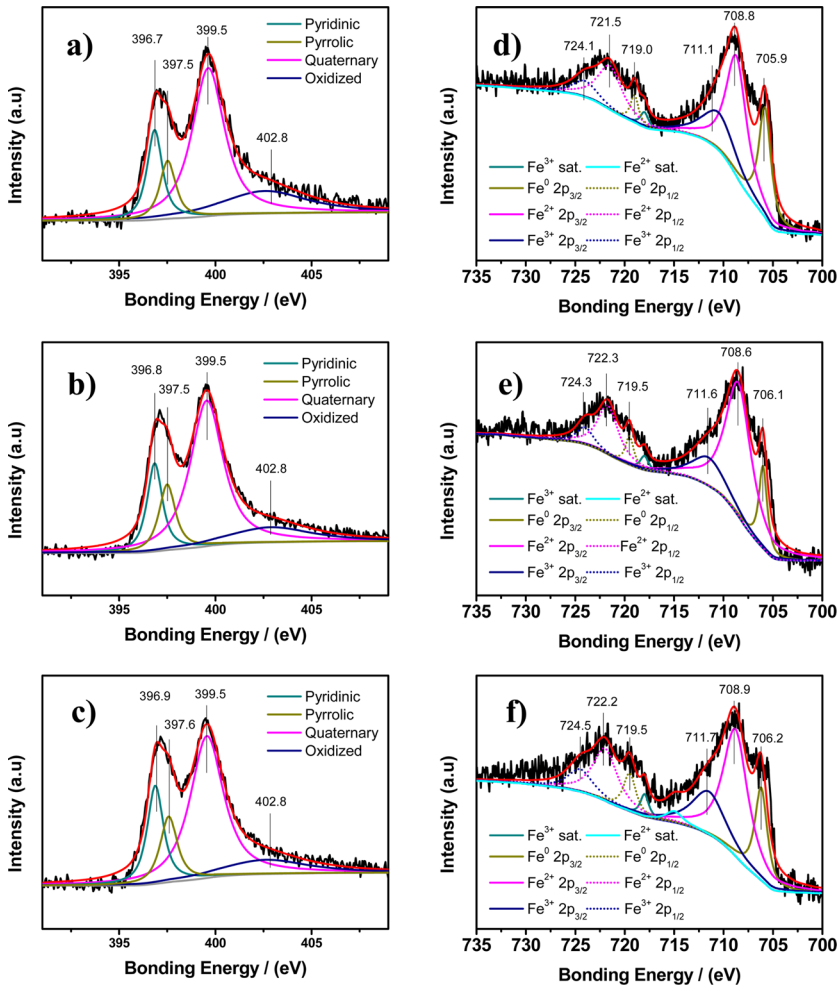

Figure 3. Fine structure of N 1s and Fe 2p XPS spectra of (a, d) S-B-NCNTs, (b, e) T-B-NCNTs, and (c, f) T-H-NCNTs.

DOI: 10.1021/acsami.5b01233
ACS Appl. Mater. Interfaces 2015, 7, 7413−7420

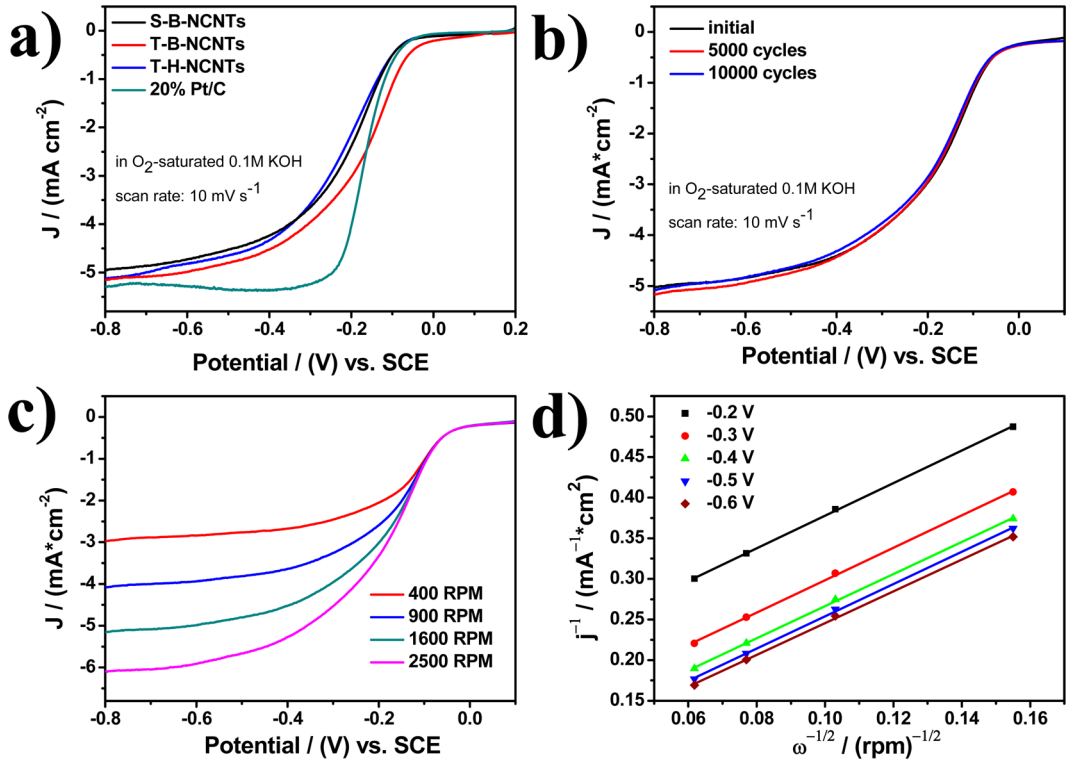

Figure 4. (a) Polarization curves of three kinds of NCNTs and Pt/C under ORR condition using a rotating disc electrode; (b) the duration test of T-B-NCNTs under ORR condition; (c) the polarization curve of T-B-NCNTs under ORR condition at different rotating speeds; (d) Koutecky–Levich plots of T-B-NCNTs at different potentials derived from RDE measurements.

hindered the application of proton exchange membrane fuel cells for large quantities of platinum must be used as catalyst. Nitrogen-doped carbon materials with excellent resist to methanol and good duration have been proven to be effective catalysts for ORR.[32] The activities toward ORR for above NCNTs were first tested via cyclic voltammetry. When nitrogen (as the protecting gas) was replaced by oxygen, the corresponding CV curve exhibited visible cathodic peaks and their peak positions depended on the kinds of NCNTs (Supporting Information Figure S5). The cathodic peaks of S-B-NCNTs, T-B-NCNTs, and T-H-NCNTs were at −0.197, −0.181, and −0.188 V vs SCE, respectively. These values are slightly negatively shifted compared with commercial Pt/C with cathodic peak at −0.165 V. Figure 3a displays the ORR activity of NCNTs and Pt/C in O_2-saturated 0.1 M KOH solution. The T-B-NCNTs showed a better overall performance toward S-B-NCNTs and T-H-NCNTs with a much higher onset potential (about 50 mV). It is even superior to commercial Pt/C. Also, T-B-NCNTs had the highest half-wave potentials of −0.17 V, which was 40 mV more positive than those of S-B-NCNTs and T-B-NCNTs, and is comparable with commercial Pt/C. However, the plateau for the diffusion controlling kinetics on the polarization curve of T-B-NCNTs is lower than commercial Pt/C, possibly because of the low exposure degree of active sites for T-B-NCNTs. The performance of T-H-NCNTs is inferior to T-B-NCNTs for there would inevitably be some residuals of the melamine foam after the pyrolysis,[22] which would cause some issues on the dispersion of the nanostructures during the activity test. It is interesting that catalysts with similar properties showed such different activities because they were not only prepared from the same precursor but also holding nearly identical nitrogen species and metal contents, which are the commonly known as the most important factors that influence the ORR activities.[32] This is probably related with iron-ligand coordination strength in the precursor.[33] As mentioned before, One of the most significant differences in the preparation procedure of S-B-NCNTs and T-B-NCNTs was that for S-B-NCNTs the iron precursor was loaded on the MgO support while for T-B-NCNTs the iron precursor was directly bonded to melamine-formaldehyde resin. During the synthesis of precursor for T-B-NCNTs, it was found that the MF resin precipitate shortly after adding $FeCl_3$ solution, forming a yellowish brown solid. The precipitation could be filtrated, leaving a solution with nearly no color. Fe^{3+} ions could not be washed away with water but be deassociated from the precursor via adding acetic acid, indicating that the metal ions did has a coordination interaction with the polymer. The FT-IR spectra of pure MF resin and Fe^{3+} coordinated MF resin changed a little at the relative attenuation of tow peaks at 1163.7 cm^{-1} (which is believed relevant to the secondary C−N vibration) and 1195.5 cm^{-1}, indicating the interaction of Fe^{3+} with the MF resin frameworks (Supporting Information Figure S6). But for the precursor of S-B-NCNTs, $FeCl_3$ is supported with MgO. Thus, there is no coordination of Fe^{3+} with MF resin. This suggests that the direct interaction of catalyst precursor, Fe^{3+}, with MF favors the formation of CNTs with higher ORR activity. The performances of different NCNTs could also be digested with comparison of the results of Fe 2p XPS in Figure 3, a larger fraction of iron species with higher valence in the form of iron carbide and/or Fe^{2+}/Fe^{3+}-N4 centers favors activity toward ORR.[31] The electrochemical durability of T-B-NCNTs was studied by an accelerated durability test. It is clear that after an accelerated lifetime test, the polarization curves is almost the same as the initial, which

DOI: 10.1021/acsami.5b01233
ACS Appl. Mater. Interfaces 2015, 7, 7413−7420

indicated that the T-B-NCNTs catalyst has an excellent electrochemical durability for ORR. The electron transfer number was calculated according to the Koutecky–Levich equation and the electron transferred during the reaction for T-B-NCNTs were 4.14, 4.17, 4.21, 4.19, and 4.25, at −0.2, −0.3, −0.4, −0.5, and −0.6 V, respectively. The average value is 4.19, demonstrating that the oxygen reduction on followed the four electrons transfer pathway.[34] The results above suggest that melamine-resin derived NCNTs could efficiently catalyze the ORR in the alkaline condition.

CONCLUSION

In summary, three kinds of nitrogen-doped carbon nanotubes were facilely synthesized via pyrolyzing melamine-formaldehyde resin with iron/iron carbide formed in situ as catalyst. The morphology of the NCNTs could be altered via adjusting the dispersion of the iron salt. Three kinds of materials contain similar nitrogen contents but different iron species. It was found that strong interaction between $FeCl_3$ and melamine-formaldehyde resin oligomers benefits the formation of iron carbide and/or Fe^{2+}/Fe^{3+}-N4 centers. All NCNTs showed good activities toward ORR, and the NCNTs derived from the precursor in which iron ions directly bonded to the polymer showed the best performance, indicating the importance of coordination interaction of nitrogen and iron before pyrolyzing procedure. The growth of the materials mainly follows a decomposition-reconstruction mechanism and we believe that the results could be adapted to other similar CVD processes involving solid precursors.

ASSOCIATED CONTENT

Supporting Information

Details of the synthesizing procedures and the figuration of electrochemical tests. This material is available free of charge via the Internet at http://pubs.acs.org.

AUTHOR INFORMATION

Corresponding Author

*E-mail: yangqh@dicp.ac.cn. Web: http://www.hmm.dicp.ac.cn; http://www.canli.dicp.ac.cn. Fax: +86 411-84694447. Tel: +86 411-84379552; +86 411-84379070.

Author Contributions

Y.Y. synthesized the materials and wrote the manuscript, B.Z. carried out the electrochemical experiments and helped write the manuscript, J.S. helped write the manuscript, and Q.Y. made the research plan, supervised the research, and organized the manuscript. The manuscript was written through contributions of all authors.

Notes

The authors declare no competing financial interest.

ACKNOWLEDGMENTS

This work was financially supported by NSFC (21325313, 21321002) and by the Key Research Program of the Chinese Academy of Sciences (Grant No. KGZD-EW-T05).

REFERENCES

(1) Iijima, S. Helical Microtubules of Graphitic Carbon. *Nature* **1991**, *354*, 56–58.
(2) Baughman, R. H.; Zakhidov, A. A.; de Heer, W. A. Carbon Nanotubes—The Route Toward Applications. *Science* **2002**, *297*, 787–792.
(3) Tasis, D.; Tagmatarchis, N.; Bianco, A.; Prato, M. Chemistry of Carbon Nanotubes. *Chem. Rev.* **2006**, *106*, 1105–1136.
(4) Pylypenko, S.; Borisevich, A.; More, K. L.; Corpuz, A. R.; Holme, T.; Dameron, A. A.; Olson, T. S.; Dinh, H. N.; Gennett, T.; O'Hayre, R. Nitrogen: Unraveling the Secret to Stable Carbon-Supported Pt-Alloy Electrocatalysts. *Energy Environ. Sci.* **2013**, *6*, 2957–2964.
(5) Rao, C. V.; Cabrera, C. R.; Ishikawa, Y. In Search of the Active Site in Nitrogen-Doped Carbon Nanotube Electrodes for the Oxygen Reduction Reaction. *J. Phys. Chem. Lett.* **2010**, *1*, 2622–2627.
(6) Lai, L.; Potts, J. R.; Zhan, D.; Wang, L.; Poh, C. K.; Tang, C.; Gong, H.; Shen, Z.; Lin, J.; Ruoff, R. S. Exploration of the Active Center Structure of Nitrogen-Doped Graphene-Based Catalysts for Oxygen Reduction Reaction. *Energy Environ. Sci.* **2012**, *5*, 7936–7942.
(7) Majeed, S.; Zhao, J.; Zhang, L.; Anjum, S.; Liu, Z.; Xu, G. Synthesis and Electrochemical Applications of Nitrogen-Doped Carbon Nanomaterials. *Nanotechnol. Rev.* **2013**, *2*, 615–635.
(8) Koziol, K.; Boskovic, B.; Yahya, N. Synthesis of Carbon Nanostructures by CVD Method. In *Carbon and Oxide Nanostructures*; Springer: Berlin, 2011; Vol. *5*, pp 23–49.
(9) Qi, H.; Qian, C.; Liu, J. Synthesis of High-Purity Few-Walled Carbon Nanotubes from Ethanol/Methanol Mixture. *Chem. Mater.* **2006**, *18*, 5691–5695.
(10) Schwenke, A. M.; Stumpf, S.; Hoeppener, S.; Schubert, U. S. Free-Standing Carbon Nanofibrous Films Prepared by a Fast Microwave-Assisted Synthesis Process. *Adv. Funct. Mater.* **2014**, *24*, 1602–1608.
(11) Tessonnier, J.-P.; Su, D. S. Recent Progress on the Growth Mechanism of Carbon Nanotubes: A Review. *ChemSusChem* **2011**, *4*, 824–847.
(12) Chung, H. T.; Won, J. H.; Zelenay, P. Active and Stable Carbon Nanotube/Nanoparticle Composite Electrocatalyst for Oxygen Reduction. *Nat. Commun.* **2013**, *4*, 1922.
(13) Terrones, M.; Terrones, H.; Grobert, N.; Hsu, W. K.; Zhu, Y. Q.; Hare, J. P.; Kroto, H. W.; Walton, D. R. M.; Kohler-Redlich, P.; Rühle, M.; Zhang, J. P.; Cheetham, A. K. Efficient Route to Large Arrays of CNx Nanofibers by Pyrolysis of Ferrocene/Melamine Mixtures. *Appl. Phys. Lett.* **1999**, *75*, 3932–3934.
(14) Maldonado, S.; Stevenson, K. J. Influence of Nitrogen Doping on Oxygen Reduction Electrocatalysis at Carbon Nanofiber Electrodes. *J. Phys. Chem. B* **2005**, *109*, 4707–4716.
(15) Yang, Xu; Tomita, A.; Kyotani, T. The Template Synthesis of Double Coaxial Carbon Nanotubes with Nitrogen-Doped and Boron-Doped Multiwalls. *J. Am. Chem. Soc.* **2005**, *127*, 8956–8957.
(16) Shi, Q.; Peng, F.; Liao, S.; Wang, H.; Yu, H.; Liu, Z.; Zhang, B.; Su, D. Sulfur and Nitrogen Co-doped Carbon Nanotubes for Enhancing Electrochemical Oxygen Reduction Activity in Acidic and Alkaline Media. *J. Mater. Chem. A* **2013**, *1*, 14853–14857.
(17) Koós, A. A.; Dowling, M.; Jurkschat, K.; Crossley, A.; Grobert, N. Effect of the Experimental Parameters on the Structure of Nitrogen-Doped Carbon Nanotubes Produced by Aerosol Chemical Vapour Deposition. *Carbon* **2009**, *47*, 30–37.
(18) Liu, H.; Zhang, Y.; Li, R.; Sun, X.; Désilets, S.; Abou-Rachid, H.; Jaidann, M.; Lussier, L.-S. Structural and Morphological Control of Aligned Nitrogen-Doped Carbon Nanotubes. *Carbon* **2010**, *48*, 1498–1507.
(19) Nagaiah, T. C.; Kundu, S.; Bron, M.; Muhler, M.; Schuhmann, W. Nitrogen-Doped Carbon Nanotubes as a Cathode Catalyst for the Oxygen Reduction Reaction in Alkaline Medium. *Electrochem. Commun.* **2010**, *12*, 338–341.
(20) Zhang, J.; Wang, R.; Liu, E.; Gao, X.; Sun, Z.; Xiao, F.-S.; Girgsdies, F.; Su, D. S. Spherical Structures Composed of Multiwalled Carbon Nanotubes: Formation Mechanism and Catalytic Performance. *Angew. Chem., Int. Ed.* **2012**, *51*, 7581–7585.
(21) Liang, J.; Zhou, R. F.; Chen, X. M.; Tang, Y. H.; Qiao, S. Z. Fe–N Decorated Hybrids of CNTs Grown on Hierarchically Porous Carbon for High-Performance Oxygen Reduction. *Adv. Mater.* **2014**, *26*, 6074–6079.

DOI: 10.1021/acsami.5b01233
ACS Appl. Mater. Interfaces 2015, 7, 7413–7420

(22) Yang, Y.; Deng, Y.; Tong, Z.; Wang, C. Multifunctional Foams Derived from Poly(Melamine Formaldehyde) as Recyclable Oil Absorbents. *J. Mater. Chem. A* **2014**, *2*, 9994−9999.
(23) Zou, X.; Huang, X.; Goswami, A.; Silva, R.; Sathe, B. R.; Mikmeková, E.; Asefa, T. Cobalt-Embedded Nitrogen-Rich Carbon Nanotubes Efficiently Catalyze Hydrogen Evolution Reaction at All pH Values. *Angew. Chem., Int. Ed.* **2014**, *126*, 4461−4465.
(24) Su, P.; Xiao, H.; Zhao, J.; Yao, Y.; Shao, Z.; Li, C.; Yang, Q. Nitrogen-Doped Carbon Nanotubes Derived from Zn−Fe−ZIF Nanospheres and Their Application as Efficient Oxygen Reduction Electrocatalysts with *in-situ* Generated Iron Species. *Chem. Sci.* **2013**, *4*, 2941−2946.
(25) Li, W.; Chen, D.; Li, Z.; Shi, Y.; Wan, Y.; Wang, G.; Jiang, Z.; Zhao, D. Nitrogen-Containing Carbon Spheres with Very Large Uniform Mesopores: The Superior Electrode Materials for EDLC in Organic Electrolyte. *Carbon* **2007**, *45*, 1757−1763.
(26) Yang, G.; Han, H.; Li, T.; Du, C. Synthesis of Nitrogen-Doped Porous Graphitic Carbons Using Nano-$CaCO_3$ as Template, Graphitization Catalyst, and Activating Agent. *Carbon* **2012**, *50*, 3753−3765.
(27) Hulicova, D.; Yamashita, J.; Soneda, Y.; Hatori, H.; Kodama, M. Supercapacitors Prepared from Melamine-Based Carbon. *Chem. Mater.* **2005**, *17*, 1241−1247.
(28) Wang, Y.; Wang, X.; Antonietti, M. Polymeric Graphitic Carbon Nitride as a Heterogeneous Organocatalyst: From Photochemistry to Multipurpose Catalysis to Sustainable Chemistry. *Angew. Chem., Int. Ed.* **2012**, *51*, 68−89.
(29) Tessonnier, J.-P.; Becker, M.; Xia, W.; Girgsdies, F.; Blume, R.; Yao, L.; Su, D. S.; Muhler, M.; Schlögl, R. Spinel-Type Cobalt−Manganese-Based Mixed Oxide as Sacrificial Catalyst for the High-Yield Production of Homogeneous Carbon Nanotubes. *ChemCatChem.* **2010**, *2*, 1559−1561.
(30) Dedryvère, R.; Maccario, M.; Croguennec, L.; Le Cras, F.; Delmas, C.; Gonbeau, D. X-Ray Photoelectron Spectroscopy Investigations of Carbon-Coated Li_xFePO_4 Materials. *Chem. Mater.* **2008**, *20*, 7164−7170.
(31) Saputro, A. G.; Kasai, H. Oxygen Reduction Reaction on Neighboring Fe-N4 and Quaternary-N Sites of Pyrolized Fe/N/C Catalyst. *Phys. Chem. Chem. Phys.* **2015**, *17*, 3059−3071.
(32) Yao, Y.; Xiao, H.; Wang, P.; Su, P.; Shao, Z.; Yang, Q. CNTs@Fe−N−C Core-shell Nanostructures as Active Electrocatalyst for Oxygen Reduction. *J. Mater. Chem. A* **2014**, *2*, 11768−11775.
(33) Tian, J.; Morozan, A.; Sougrati, M. T.; Lefèvre, M.; Chenitz, R.; Dodelet, J.-P.; Jones, D.; Jaouen, F. Optimized Synthesis of Fe/N/C Cathode Catalysts for PEM Fuel Cells: A Matter of Iron−Ligand Coordination Strength. *Angew. Chem., Int. Ed.* **2013**, *52*, 6867−6870.
(34) Peng, H.; Mo, Z.; Liao, S.; Liang, H.; Yang, L.; Luo, F.; Song, H.; Zhong, Y.; Zhang, B. High Performance Fe- and N-Doped Carbon Catalyst with Graphene Structure for Oxygen Reduction. *Sci. Rep.* **2013**, *3*, 1765.

DOI: 10.1021/acsami.5b01233
ACS Appl. Mater. Interfaces 2015, 7, 7413−7420